A SEMI-NUMERICAL METHOD FOR ELASTIC WAVE SCATTERING CALCULATIONS

Ajit Mal
Mechanical and Aerospace Engineering Department
University of California
Los Angeles, CA 90095-1597
Tel: 310-825-5481, Fax: 310-206-4830, e-mail: ajit@ucla.edu
Current address:
Mechanical Engineering Department
Etcheverry Hall #1740
University of California
Berkeley, CA 94720-1740
Tel: 510-642-9632
and

Zensheu Chang
Jet Propulsion Laboratory, California Institute of Technology
Mail Stop 67-119
Pasadena, California 91109

Abstract. This paper is concerned with the calculation of elastic wavefields in strongly heterogeneous media containing scatterers of arbitrary shape and size. A hybrid method is described in which the elastodynamic field within a finite region enclosing the scatterers is modeled by finite elements while the field away from this region is represented by means of a suitable set of wavefunctions. Application of a variational principle and the continuity conditions at the interface between the two regions lead to a system of linear equations that is solved by standard techniques. The hybrid method extends the applicability of the finite element method to wave propagation problems in unbounded media by rigorously modeling the radiation field. The method is used to calculate of the elastodynamic field in a plate of finite thickness and infinite lateral dimensions containing geometric discontinuities.

Introduction. Calculation of elastic wavefields in heterogeneous media is of great interest in a variety of applications including strong ground motion simulation for earthquake resistant design, seismic tomography to determine the earth's internal constitution, nondestructive evaluation to detect and characterize flaws in critical structural components, etc. There is a vast amount of literature on the interaction of elastic waves with single as well as multiple inhomogeneities and no attempt will be made to it here. It should be noted that asymptotic theories valid at low or high frequencies have been the mainstay of early work on the subject and they have provided valuable physical insight into the qualitative features of the interaction phenomena. However the asymptotic techniques lose their accuracy in the intermediate frequency range where the interaction effects are most pronounced more interesting and more useful for practical applications. Analytical techniques that can be applied in the entire frequency range are limited to relatively simple geometry of the scatterers, e.g., cylinders and spheres [see e.g., Knopoff, 1959a,b; Gilbert and Knopoff, 1959, 1961; Mal and Bose, 1974; Yang and Mal, 1994]. Modern applications require the availability of calculation models that can simulate wave interaction phenomena in media containing scatterers of arbitrary shape and size at all frequencies.

Although the finite element method (FEM) provides a convenient and powerful means for representing the inhomogeneous region, its conventional implementation presents difficulty in modeling the radiated field external to the discretized region. An alternative procedure is to employ a time domain formulation in a finite region if the interest is limited to small time windows. However, the observed dissipative properties of most materials indicate that it is difficult, if not impossible to express their constitutive equations in the time domain. Thus, for calculations that are valid for large time windows and where the dissipative properties of the materials are significant, the frequency domain formulation is preferable. Other potentially useful semi-numerical methods include the boundary integral equation method [see, e.g., Dravinski, 1984] and the volume integral equation method [Mal and Knopoff, 1967; Lee and Mal, 1995].

In what follows a recently developed hybrid technique incorporating the widely used finite element method (FEM) near the inhomogeneity and analytical representation of the wave functions in the far field is described. The hybrid technique can extend the range of application of FEM to unbounded media without the need to discretize large regions [see, e.g., Goetschel, Dong and Muki, 1982]. In this paper the hybrid method is applied to the problem of a plate containing geometrical discontinuities as an illustrative example.

The interaction of Lamb waves with a free edge of a plate was first studied by Torvik [1967], where a variational technique was used to derive the modal coefficients. In addition, the partition of energy between different modes above the first cutoff frequency was studied. Using the projection method, Gregory and Gladwell [1983] studied the free edge reflection problem and extended the frequency range investigated by Torvik [1967]. In both cases, the first symmetric mode Lamb wave was used as the incident wave. The anti-symmetric case was not considered in either study. The conventional FEM was applied to plates with defects by Alleyn and Cawley [1992], and a hybrid method was used by Datta, Al-Nassar and Shah [1991] to calculate the waves scattered by a crack within a plate. In this paper the two-dimensional (in-plane) problem of Lamb wave propagation in a plate of finite thickness and infinite lateral dimensions containing defects on one of its surfaces is considered. A three dimensional problem of the plate has been considered in Chang and Mal [1999].

The Hybrid Technique. The geometry of the general problem is depicted in Fig. 1, where the material (henceforth referred to as the *inclusion*) bounded by the surface S has significantly different properties from that outside S (the *matrix*). The inclusion itself can be heterogeneous, anisotropic and viscoelastic. The matrix is assumed to be homogeneous, isotropic and

Figure 1. The hybrid model of the general wave scattering problem.

viscoelastic for the sake of simplicity. The waves are assumed to be generated by sources external to the inclusion.

Let $\boldsymbol{u}(\boldsymbol{x}, \omega)$ denote the Fourier time transform of the displacement vector at a point $\boldsymbol{x}$ within the solid. Then $\boldsymbol{u}(\boldsymbol{x}, \omega)$ is, in general, a complex, frequency dependent function and is the solution of a time harmonic boundary value problem in which all field variables have the time dependence $e^{-i\omega t}$. The time domain solution can be easily obtained through inversion using FFT or other suitable algorithms. In what follows we consider time harmonic problems only, and suppress the common time dependence as well as the frequency dependence in all field variables. The Cartesian components of the stress tensor, τ, are related to the components of the displacement through the appropriate constitutive equation. The displacement vector $\boldsymbol{u}$ satisfies Navier's equations and is continuous everywhere except at the source. The stress vector is continuous across all surface elements including those where a sharp transition in material properties may occur. In addition, for an unbounded matrix, the field must represent outgoing waves or satisfy a radiation condition at infinity.

In order to illustrate the frequency-domain hybrid method for unbounded media, assume that a plane time harmonic wave is incident on the irregularly shaped inclusion perfectly bonded to the matrix at the interface S, and introduce a surface B containing the inclusion as the FEM mesh boundary. The region inside B is discretized and analyzed by the finite element method and the behavior of the region outside B is represented by a set of *global wave functions*. The continuity of the displacement and traction on the mesh boundary must be satisfied through proper choice of the amplitudes of the global functions.

The global functions are the displacements which satisfy the governing equation and the boundary conditions of the same problem in absence of the inclusion, and will be denoted by $\mathbf{g}_n$ (n =1, 2,...). Assume that the displacements associated with the incident wave $\mathbf{u}^I$ and the scattered wave $\mathbf{u}^S$ outside S can be expressed in the forms

$$\boldsymbol{u}^I = \sum_{n=1}^{p} a_n \boldsymbol{g}_n \qquad (1a)$$

$$\boldsymbol{u}^S = \sum_{n=1}^{q} b_n \boldsymbol{g}_n \qquad (1b)$$

where p, q are integers to be selected based on needed accuracy, the constants a_n are known, and the constants b_n are to be determined from the continuity conditions on the mesh boundary. The finite element formulation is based on the minimization of the functional

$$\Pi = \int_V \left(\rho\omega^2 u_i u_i^* - \frac{\tau_{ij} u_{i,j}^*}{2} + f_i u_i^* \right) dV + \int_S \tau_{ij} u_i^* n_j \, dS \qquad (2)$$

where ρ is the density of the material, a superstar implies complex conjugation, $\boldsymbol{f}$ is the body force and $\boldsymbol{n}$ is the unit normal vector to S. In the conventional finite element technique, either the displacement u_i or the stress vector $\tau_{ij}n_j$ is prescribed on S, but the boundary conditions for the present problem are of a different type, as will be seen below.

Using the conventional finite element discretization of the field inside the mesh boundary, B, and applying the variational principle based on the minimization of (2), a system of linear equations relating the nodal displacements to the nodal forces is obtained. For convenience, we divide both the displacement and the force vectors into two parts: one part is associated with the nodes interior to the mesh boundary, the other part is for the boundary nodes. The linear equations can be expressed in block matrix notation as follows:

$$\begin{bmatrix} D_{ii} & D_{ib} \\ D_{bi} & D_{bb} \end{bmatrix} \begin{Bmatrix} U_i \\ U_b \end{Bmatrix} = \begin{Bmatrix} F_i \\ F_b \end{Bmatrix} \tag{3}$$

where the subscript b refers to the boundary, and the subscript i refers to the interior, $\{U\}$ is the column vector of the nodal displacements and F is the column vector of the nodal forces. The matrix $[D_{ii}]$ relates the interior nodal displacements to the interior nodal forces, $[D_{bb}]$ relates those on the boundary, $[D_{ib}]$ and $[D_{bi}]$ are the coupling matrices between the interior and boundary nodes.

For the time being, we only consider the field variables at the nodes on the mesh boundary. From (1b), we may derive the values of both the displacement and the force vectors corresponding to the incident wave at the nodes on the mesh boundary, by substituting the coordinates of the boundary nodes into the global functions. Thus

$$\left\{U_b^I\right\} = \sum_{n=1}^{p} a_n \left\{G_n\right\} \tag{4}$$

$$\left\{F_b^I\right\} = \sum_{n=1}^{p} a_n \left\{F_n\right\} \tag{5}$$

where $\{G_n\}$ is the vector composed of the values of the global functions $\boldsymbol{g_n}$ on the mesh boundary, and $\{F_n\}$ is the associated force vector.

Using each displacement vector $\{G_n\}$ in (4) as the boundary condition on S, and by the conventional finite element approach, we obtain the corresponding boundary forces:

$$\left\{F_b^I\right\}_{FEM} = \sum_{n=1}^{p} a_n \left\{V_{nb}\right\} \tag{6}$$

where the vector $\{V_{nb}\}$ is the result of using the displacement vector $\{G_n\}$ in (4) as the boundary condition. The subscript "FEM" implies that the vector is derived from the interior finite element.

Similarly, we may derive the displacement and force vectors associated with the scattered field:

$$\left\{U_b^S\right\} = \sum_{n=1}^{q} b_n \left\{G_n\right\} \tag{7}$$

$$\left\{F_b^S\right\} = \sum_{n=1}^{q} b_n \left\{F_n\right\} \tag{8}$$

$$\left\{F_b^S\right\}_{FEM} = \sum_{n=1}^{q} b_n \left\{V_{nb}\right\} \tag{9}$$

Clearly the displacement continuity across the mesh boundary is automatically satisfied, since we have used the displacement vectors derived from the global functions as the boundary conditions for the discretized region. Thus the only continuity condition that remains to be satisfied is the nodal force condition. There are two sets of force vectors on the mesh boundary, one from the global functions, the other from the finite element model; each set contains both the incident and the scattered parts. The next step is to find a set of unknown amplitudes b_n which minimizes the difference between the two force vectors. Equating the boundary nodal force vectors from the global functions to those from the finite element method, we obtain

$$\begin{aligned}\{F_b^I\}+\{F_b^S\} &= \sum_{n=1}^{p} a_n\{F_n\}+\sum_{n=1}^{q} b_n\{F_n\} \\ &= \{F_b^I\}_{FEM}+\{F_b^S\}_{FEM} = \sum_{n=1}^{p} a_n\{V_{nb}\}+\sum_{n=1}^{q} b_n\{V_{nb}\}\end{aligned} \tag{10}$$

This leads to a system of linear equations for b_n of the form

$$\sum_{n=1}^{q} b_n\left(\{F_n\}-\{V_{nb}\}\right)=\sum_{n=1}^{p} a_n\left(\{V_{nb}\}-\{F_n\}\right) \tag{11}$$

which can be expressed in matrix form as

$$[A]_{m\times q}\{b\}_{q\times 1}=\{c\}_{m\times 1} \tag{12}$$

In (12) the elements of the matrix $[A]$ and the vectors $\{b\}$ and $\{c\}$ are all complex, m is the total number of nodes on the mesh boundary, and q is the total number of global functions used to represent the scattered field. Since m is usually greater than q, the unknowns b_n can be solved by applying the least square method, which minimizes the difference between the left and right hand sides of (12). This is equivalent to minimizing the difference between the displacement fields just inside and just outside the mesh boundary. This minimization leads to the standard linear system

$$\left([A^*]^T_{q\times m}[A]_{m\times q}\right)\{b\}_{q\times 1}=[A^*]^T_{q\times m}\{c\}_{m\times 1} \tag{13}$$

where the superstar indicates complex conjugate, and the superscript T indicates a transpose. Once the global functions are known the system of equations (13) can be solved by means of standard techniques. The hybrid formulation has been applied to the solution of problems of special interest in the inspection of aging aircraft structures involving Lamb wave propagation in a plate with geometric discontinuities. Representative results are presented below.

The Global Functions for the Plate. For the plate Lamb waves are used as the global functions. In the two-dimensional case the motion due to Lamb waves can be decomposed into *symmetric* and *antisymmetric* modes. The displacement components U and V associated with the two modes in the plate occupying the region $-\infty < x < \infty$, $-H < y < H$, (Fig. 2) can be expressed in the following form (see, e.g., Mal and Singh, 1991):

Symmetric Mode

$$\begin{aligned}U(x,y) &= \left[ik\cosh(\eta_1 y)-\eta_2 C\cosh(\eta_2 y)\right]e^{ikx} \\ V(x,y) &= \left[\eta_1\sinh(\eta_1 y)+ikC\sinh(\eta_2 y)\right]e^{ikx}\end{aligned} \tag{14}$$

where

$$C=-\frac{(2k^2-k_2^2)\cosh(\eta_1 H)}{2ik\eta_2\cosh(\eta_2 H)} \tag{15}$$

$$\eta_j = \sqrt{k^2 - k_j^2}, \qquad |k| > k_j$$
$$= i\sqrt{k_j^2 - k^2}, \qquad |k| < k_j \tag{16}$$
$$k_j = \frac{\omega}{c_j}, \qquad j = 1,2$$

c_1 and c_2 are the P and S-wave speeds in the solid. The associated dispersion equation is

$$\frac{\tanh(\eta_1 H)}{\tanh(\eta_2 H)} = \frac{(2k^2 - k_2^2)^2}{4k^2\eta_1\eta_2} \tag{17}$$

Antisymmetric Mode

$$U(x,y) = \left[ik\sinh(\eta_1 y) - \eta_2 D\sinh(\eta_2 y)\right]e^{ikx}$$
$$V(x,y) = \left[\eta_1\cosh(\eta_1 y) + ikD\cosh(\eta_2 y)\right]e^{ikx} \tag{18}$$

Figure 2. The geometry of the plate.

where

$$D = -\frac{(2k^2 - k_2^2)\sinh(\eta_1 H)}{2ik\eta_2\sinh(\eta_2 H)} \tag{19}$$

The associated dispersion equation is

$$\frac{\tanh(\eta_2 H)}{\tanh(\eta_1 H)} = \frac{(2k^2 - k_2^2)^2}{4k^2\eta_1\eta_2} \tag{20}$$

The global function $\mathbf{g_n}$ is the vector {U, V} calculated at $k = k_n$, where k_n is the n-th root of the dispersion equation (17) or (20). The expressions for the global function given in (14) and (18) are valid on the right hand side of the mesh. For the left hand side of the mesh, the global functions are simply $\mathbf{g_n}^*$, the complex conjugate of $\mathbf{g_n}$. It should be noted that the roots of (17) and (20) may be real or complex. At a given frequency, these equations have a finite number of real roots and an infinite number of pure imaginary or complex roots. The real roots are associated with the propagating modes; their amplitude remains constant at points away from the source. The complex roots are associated with nonpropagating modes; their amplitude decays exponentially with distance from the source. In the present problem, the geometrical boundaries of the defects act as virtual sources for both propagating and nonpropagating waves. In the vicinity of the defects, the contribution to the wavefield from the two types of waves are comparable, but the relative strength of the nonpropagating modes decreases away from the defects. It has been shown by Vasudevan and Mal (1985), that the effect of the nonpropagating modes can be ignored at points about twice the plate thickness away from the source. Thus if the mesh boundary is located at least twice the plate thickness away from the defects, the nonpropagating modes can be ignored outside the mesh boundary and only the propagating modes can be used as the global functions. The material properties of the plate used in the numerical calculation are shown in Table 1, and the dispersion curves for symmetric and antisymmetric Lamb waves are shown in Fig. 3. .

Table 1. The properties of the aluminum plate used in the numerical calculations.

Thickness, 2H (mm)	P-wave speed, c_1 (Km/sec)	S-wave speed, c_2 (Km/sec)	Density ρ (g/cc)
1.6	6.4	3.1	2.8

It should be noted that at a fixed frequency there are a small number of propagating modes and an additional mode is added at each cutoff frequency.

Lamb waves in plates with defects

In order to illustrate the application of the hybrid technique to wave scattering problems, the propagation of Lamb waves in a semi-infinite plate with a surface defect under plane strain conditions is considered next. The plate is divided into two parts by the mesh boundary as shown in Fig. 4. The region between the mesh boundary and the free edge of the plate is analyzed by the finite element method, while the behavior of waves in the semi-infinite plate on the left side of the mesh boundary is represented by the Lamb wave modal expansion. Application of the continuity conditions across the mesh boundary leads to a system of over-determined, complex, linear equations, which is solved by the least square method. The mesh boundary is located at a distance of ten times the plate thickness away from the free edge. The fundamental symmetric (S_0) and anti-symmetric (A_0) modes are used as incident waves.

We first present some of our calculated results in absence of the defect. The fundamental symmetric (S_0) and anti-symmetric (A_0) modes are used as incident waves. Clearly, an incident symmetric mode is reflected as symmetric modes only and an anti-symmetric mode is reflected

Fig. 4. The hybrid model of the plate with a surface defect.

as anti-symmetric modes. Moreover, in the frequency range below the first cutoff frequency (approximately, 0.97MHz for the antisymmetric mode and 1.48 MHz for the symmetric mode), only the corresponding fundamental mode is reflected, and the amplitude is the same as that of the incident wave. However, at higher frequencies, higher modes are induced in addition to the fundamental mode, and the global functions must include an adequate number of these modes. The number of modes to be included depends on the frequency range of interest. As an example, if the incident wave is the S_0 mode, and then $p = 1$, and q is the number of possible modes at the maximum frequency of interest.

The real and imaginary parts of the vertical displacement on the top surface calculated by means of the hybrid method for both symmetric and anti-symmetric cases at low frequencies are shown in Fig. 5. At these frequencies, the displacement is pure imaginary for the symmetric case, as shown in the figure, while for the anti-symmetric case the real and imaginary parts of the displacement are equal. Both of these cases represent standing waves within the plate. It can also be seen that for the anti-symmetric case, the displacement is larger at the free edge and becomes sinusoidal at distances away from the free edge. This is because the non-propagating modes are also induced when the incident wave strikes the free edge; their influence decreases away from the edge. In contrast the displacement at the free edge is almost nonexistent in the symmetric case. This is because the symmetric non-propagating modes have very little effect on the

reflected field and the incident and reflected propagating modes cancel each other at the free edge.

The real and imaginary parts of the reflected waves are plotted in Fig. 6. It can be seen that at frequencies below the first cutoff, the symmetric reflected waves suffer a phase reversal as compared to the incident wave. For the anti-symmetric case, the phase shift is 90°, but it changes

Fig. 5. The normal surface displacement calculated from the hybrid method

rapidly near the first cutoff frequency of 0.97 MHz. Similar rapid change in phase occurs in the symmetric case at 1.48 MHz, the corresponding cutoff frequency. These effects have also been observed by Torvik [1967] in the symmetric case. An interesting feature of the solution is the behavior of the waves at the cutoff frequencies. The vertical displacement at the symmetric

Fig. 6. Real and imaginary parts of the surface displacements due to the reflected waves.

resonant frequency of 1.48 MHz is shown in Fig. 7. It can be seen that the displacement at the free edge is about 7 times higher than that away from the free edge.

The semi-infinite plate with surface defects is considered next. Defects of various widths and depths are introduced at the top surface of the plate. The fundamental symmetric mode is used as

Fig. 7. Top surface displacement at the cutoff frequency, 1.48 MHz; symmetric case.

the incident wave; the waveform is assumed to consist of a train of cosine waves modulated by a Gaussian envelope. The reflected waveforms calculated from the hybrid method are shown in Figs. 8 and 9. It can be seen that the depth of the defect has a stronger effect on the reflection than the width.

All reflections have one feature in common; the reflected signal can be roughly divided into three parts: the first part is the reflection from the defect, the second part is the wave transmitted across the defect, then reflected by the free edge and propagating across the defect again to the transducer. The last part is the wave reflected by the free edge twice and then propagating across the defect. Theoretically, an infinite number of wave trains are reflected

Fig. 8. The normal surface displacement due the incident and reflected waves for a wide and shallow defect. H = 1.6 mm.

Fig. 9. The normal surface displacement due the incident and reflected waves for a narrow defect. H = 1.6 mm.

between the defect and the free edge. All except the three signals described above are too small to be identified in the received signal, since only a very small portion of the energy is reflected each time the wave comes across the defect.

It should be noted that in both figures 8 and 9, the reflected waves have larger amplitude than the incident waves. The increase in amplitude is caused by the interference between the reflected waves from the right edge of the plate and the defect. In order to verify that the amplitude increase in the reflected field does not violate the energy principle, the energy flux through a vertical surface S_1 (x = constant) associated with the waves are calculated from the formula

$$E_f = -\frac{\omega}{2}\int_{S_1} \tau_{i1} u_i^* dS$$

The energy flux for each wave normalized to that in the incident wave is shown in Figs. 10 and 11. It can be seen that the total energy flux is unity in both cases, implying that the energy is conserved. The results also show that when the symmetric incident waves are reflected from the free edges with defects, most of the energy remains in the symmetric mode; only a small portion is converted into antisymmetric mode.

Concluding remarks. The hybrid technique described in this paper is a rigorous extension of the conventional finite element method to wave propagation problems in extended media. It takes full advantage of the capability of the conventional finite element method in modeling complex media and uses the classical analytical solutions of canonical problems to remove the difficulty associated with the FEM in modeling the radiated field. In addition to the plate problems discussed here, the method can be applied to wave propagation problems in laterally heterogeneous layered earth models.

Fig. 10. The energy flux across a vertical surface in the plate with the wide defect.

Fig. 11. The energy flux across a vertical surface in the plate with the narrow defect.

References.

Alleyne, D.N. and Cawley, P., "The Interaction of Lamb Waves with Defects", *IEEE Trans. on Ultrasonics, Ferroelectrics, and Frequency Control*, Vol. 39, pp. 381-397, 1992.

Chang, Z and Mal, A., "Scattering of Lamb Waves from a Rivet Hole with Edge Cracks", *Mechanics of Materials*, Vol. 31, pp. 197-204, 1999.

Datta, S.K., Al-Nassar, Y. and Shah, A.H., "Lamb Wave Scattering by a Surface-Breaking Crack in a Plate", *Rev. of Progress in Quantitative NDE*, Vol. 10A, D. O. Thompson and D. E. Chimenti, Eds. New York: Plenum, pp. 79-104, 1991.

Dravinski, M., "Evaluation of strong ground motion using boundary integral equation approach," in Earthquake Source Modeling, Ground Motion and Structural Response, S.K. Datt, ed., ASME-AMD-Vol. 60, pp. 61-80, 1984.

Gilbert, J.F., and Knopoff, L., "Scattering of impulsive elastic waves by a rigid cylinder," *J. Acoust. Soc. Amer.*, Vol. 31, pp. 1169-1175, 1959.

ibid, "Diffraction of elastic waves by the core of the earth," *Bull. Seismol. Soc. Amer.*, Vol. 51, pp. 35-39, 1961.

Goetschel D.B., Dong S.B. and Muki R., A Global Local Finite Element Analysis of Axisymmetric Scattering of Elastic Waves, *J. Appl. Mech.*, Vol. 49, pp. 816-820, 1982.
Gregory, R.D. and Gladwell, I. "The Reflection of a Symmetric Rayleigh-Lamb Wave at the Fixed or Free Edge of a Plate", *J. Elasticity*, Vol. 13, pp. 185-206, 1983.
Knopoff, L., "Scattering of compression waves by spherical obstacles," *Geophysics*, Vol. 24, pp. 30-39, 1959a.
ibid, "Scattering of shear waves by spherical obstacles," *Geophysics*, Vol. 24, pp. 209-219, 1959b.
Lee, J.-K . and Mal, A.K., "A Volume Integral Equation Technique for Multiple Scattering Problems in Elastodynamics", *Applied Mathematics and Computation*, Vol. 67, pp. 135-159, 1995.

Mal A.K. and Knopoff L., Elastic wave velocities in two component systems, *J. Inst. Math Applics.*, Vol. 3, pp. 376-387, 1967.
Mal, A.K., Bose, S.K. "Dynamic Elastic Moduli of a Suspension of Imperfectly Bonded Spheres," *Proc. Camb. Phil. Soc.*, Vol. 76, pp. 587-600, 1974.

Mal, A.K. and Singh, S.J., *Deformation of Elastic Solids*, Prentice-Hall, 1991.
Torvik, P.J., "Reflection of Wave Trains in Semi-Infinite Plates", *J. Acoust. Soc. Am.*, Vol. 41, pp. 346-353, 1967.
Vasudevan, N. and Mal, A.K., "Response of an Elastic Plate to Localized Transient Sources", *J. Appl. Mech.*, Vol. 107, pp. 356-362, 1985.

Yang, R.-B., and Mal, A.K., "Multiple Scattering of Elastic Waves in a Fiber-Reinforced Composite", *J. Mech. and Phys. Solids*, Vol. 42, pp. 1945-1968, 1994.

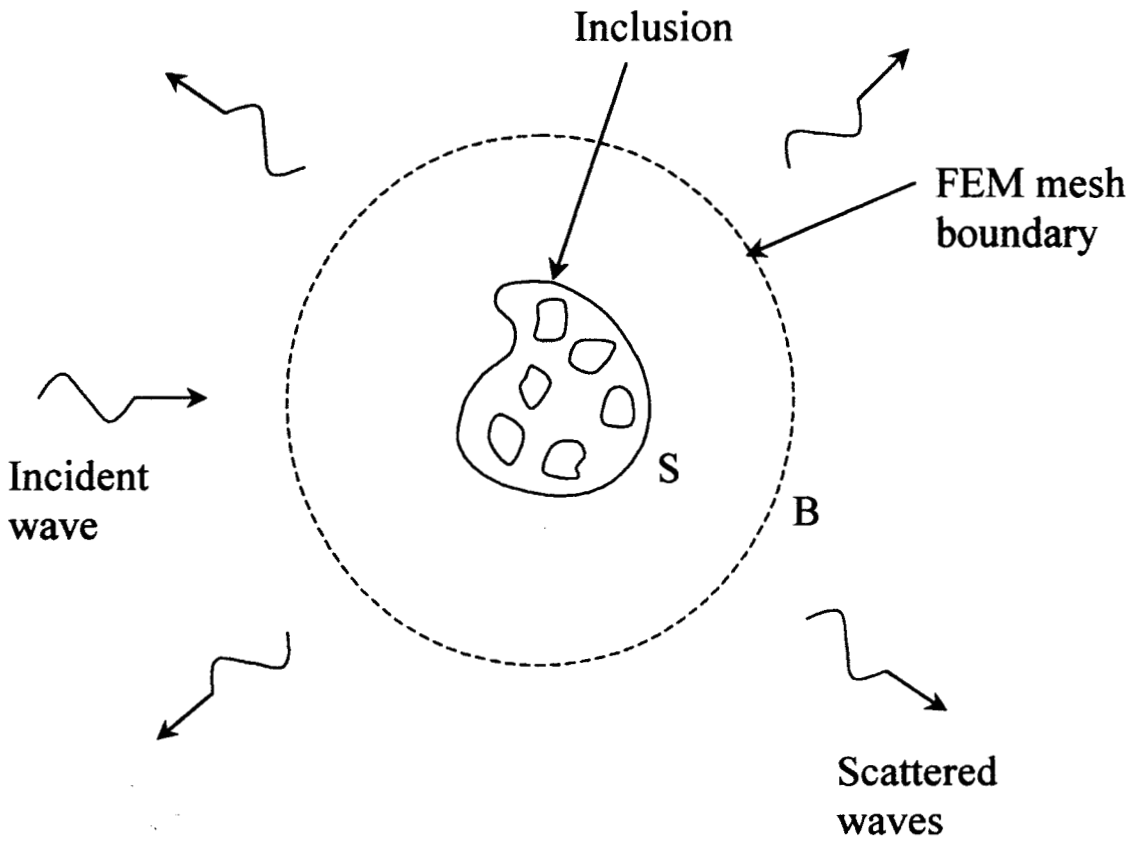

Figure 1. The hybrid model of the general wave scattering problem.

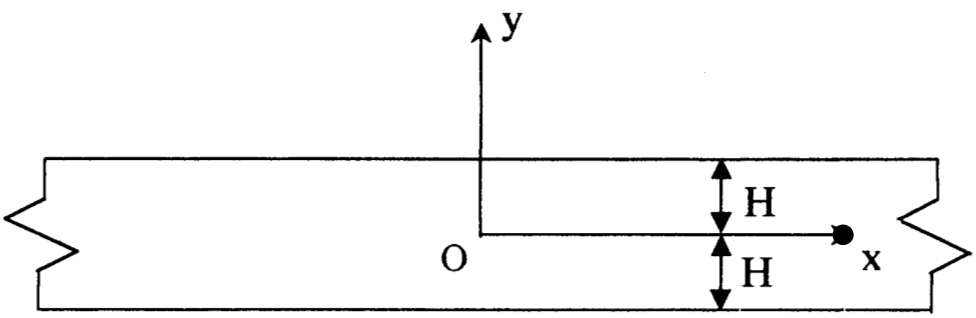

Figure 2. The geometry of the plate.

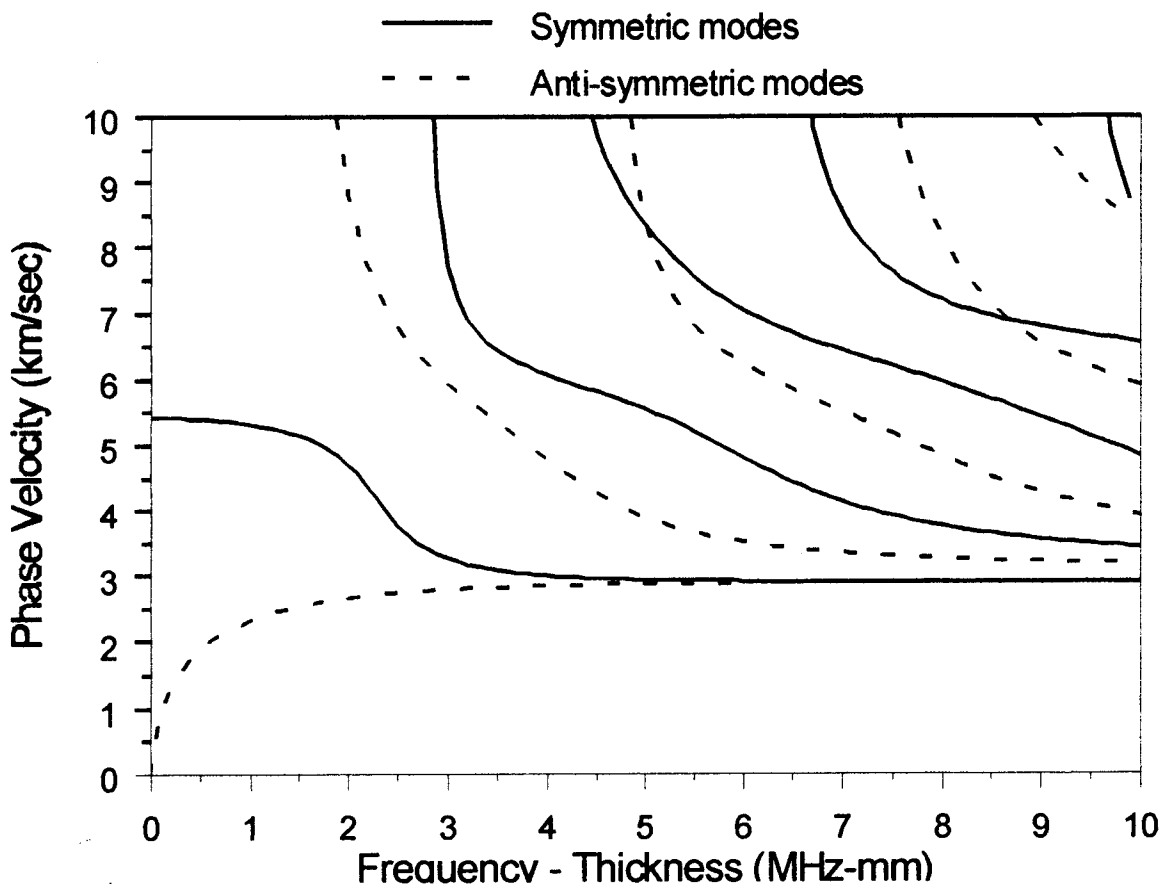

Figure 3. Lamb wave dispersion curves.

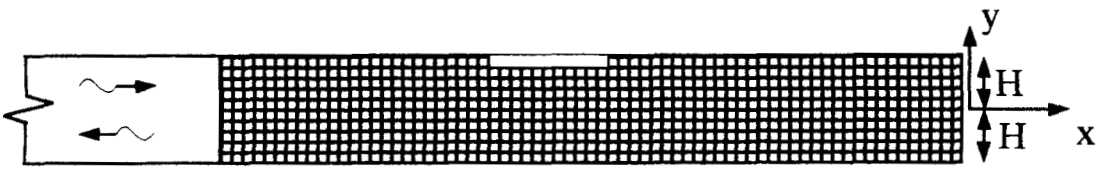

Figure 4. The hybrid model of the plate with a surface defect.

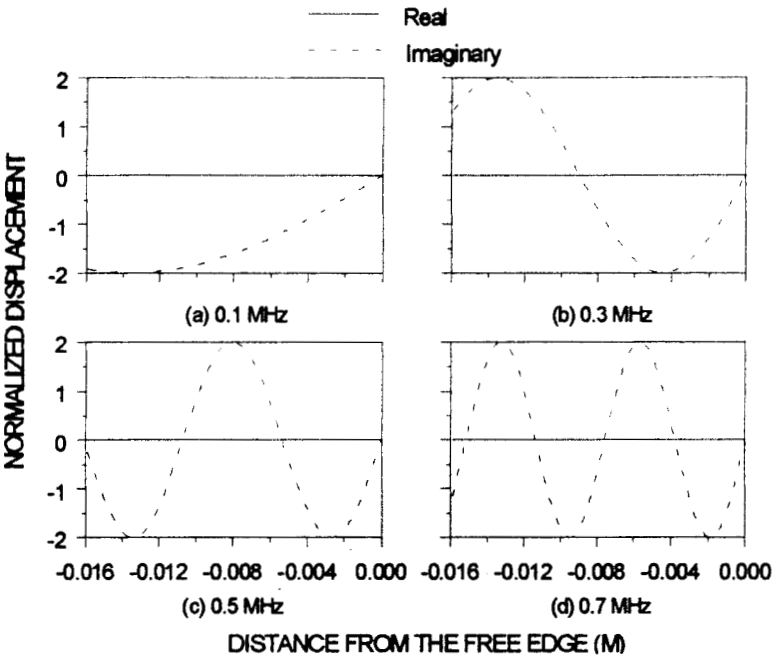

(a) symmetric case.

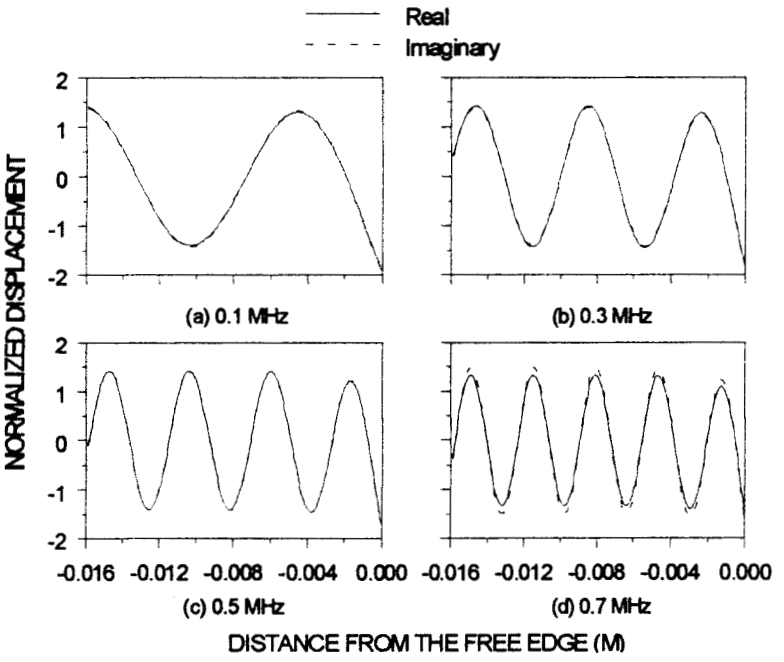

(b) antisymmetric case.

Figure 5. Real and imaginary parts of the surface displacement calculated from the global-local finite element method.

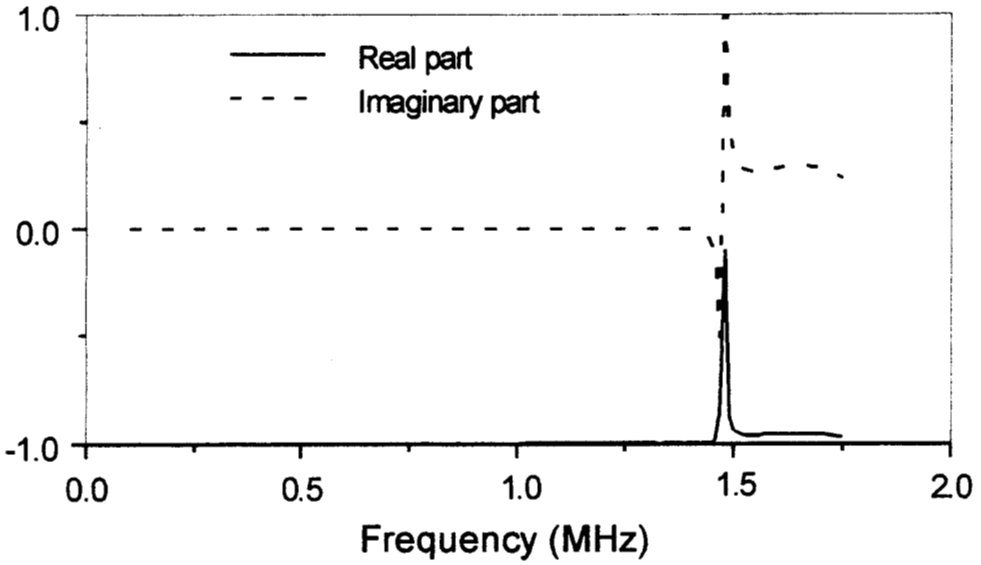

(a) Symmetric case, the first cutoff frequency is about 1.48 MHz.

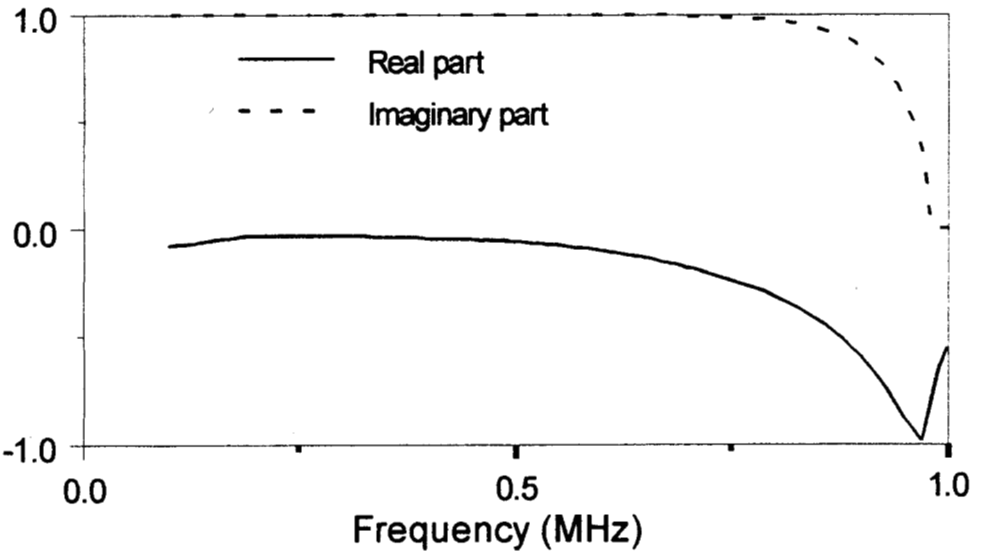

(b) Anti-symmetric case, the first cutoff frequency is about 0.97 MHz.

Figure 6. Real and imaginary parts of the surface amplitude of the reflected waves.

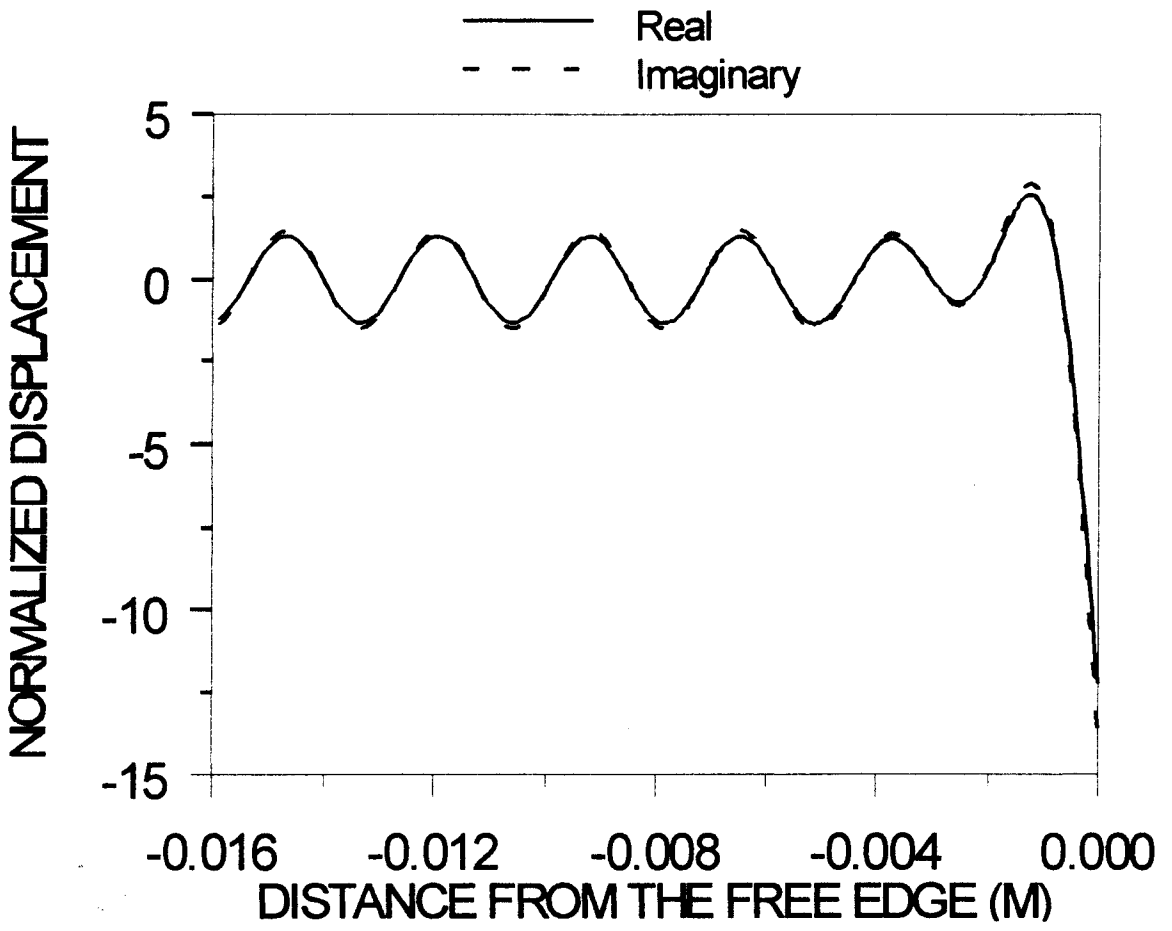

Figure 7. Top surface displacement at the cutoff frequency 1.48 MHz, symmetric case.

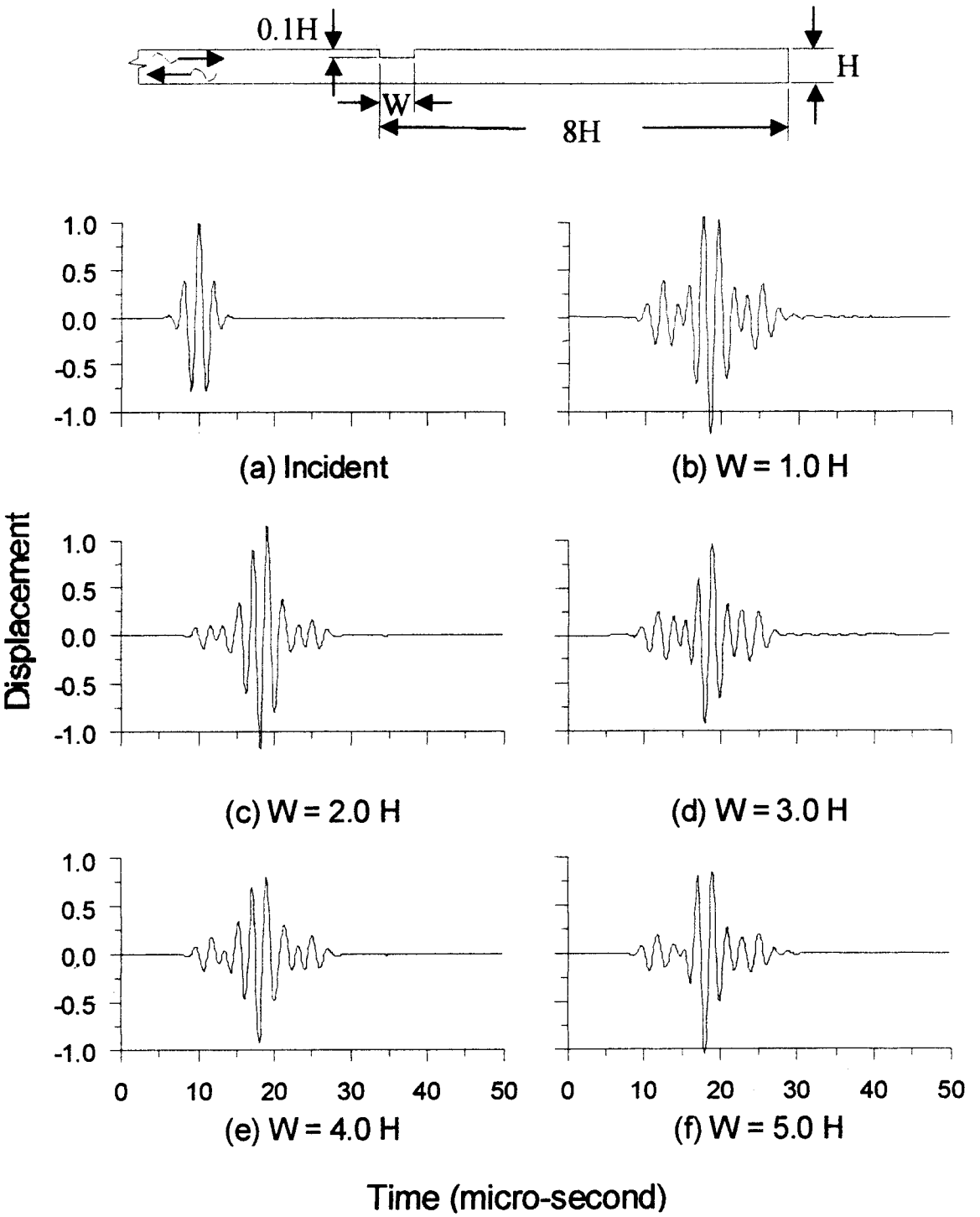

Figure 8. Displacement due to the incident and reflected waves from a wide surface defect. (H = 1.588 mm)

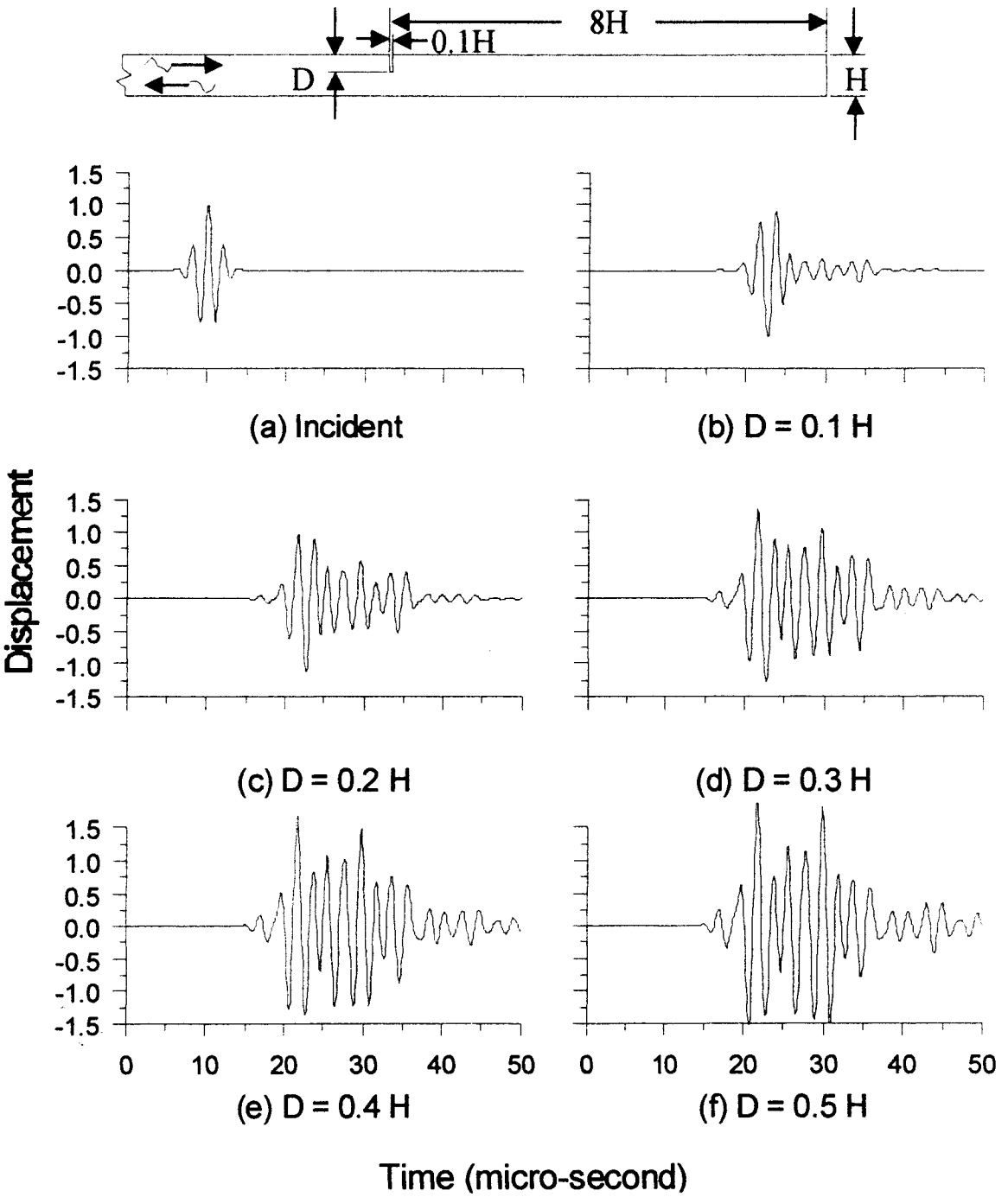

Figure 9. Displacement due to the incident and reflected waves from a narrow surface defect. (H = 1.588 mm)

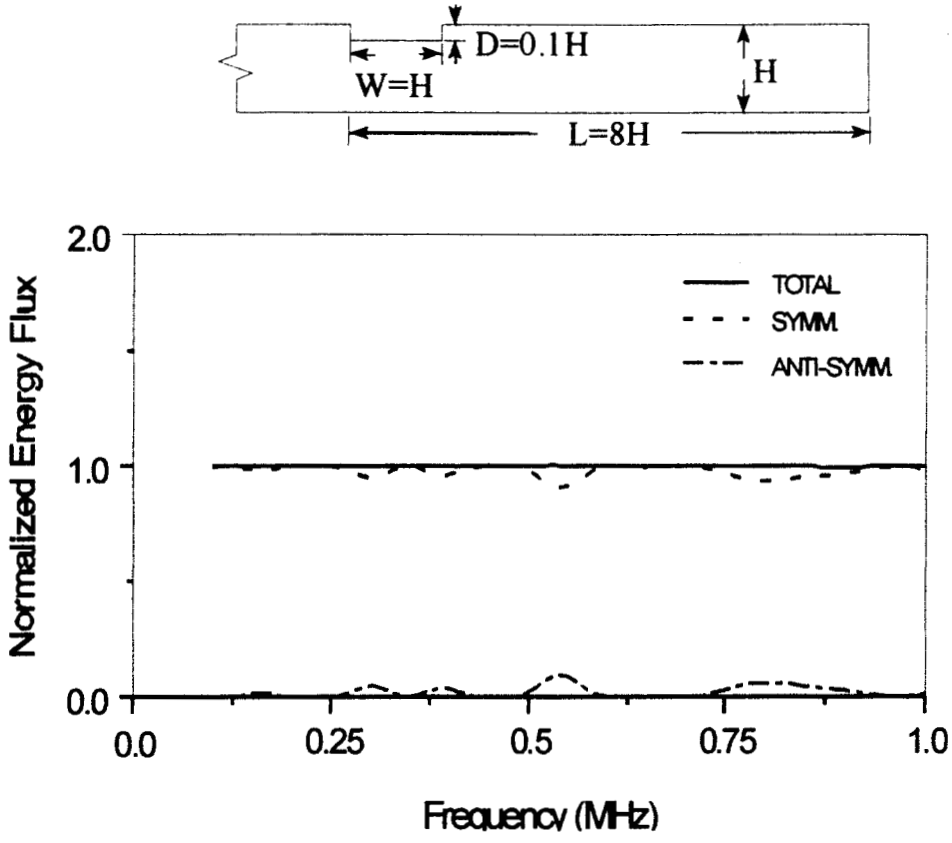

Figure 10. Partition of energy in various reflected modes for a wide surface defect.

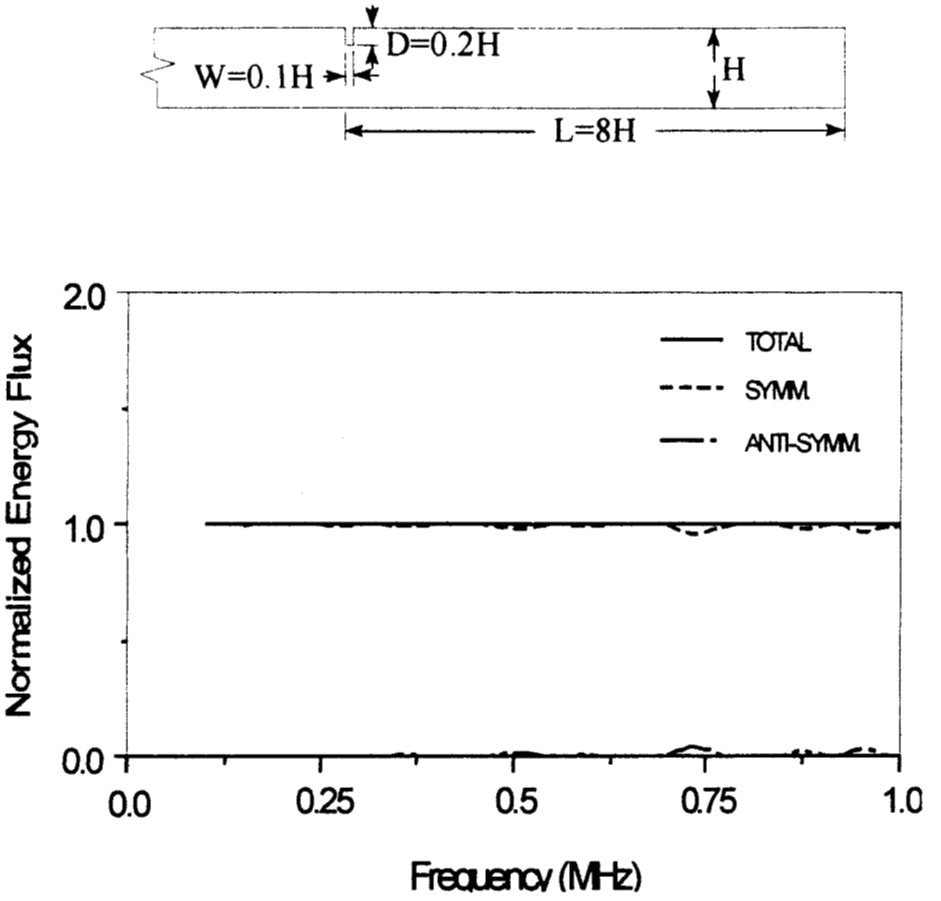

Figure 11. Partition of energy in various reflected modes for a narrow surface defect.